Determination of the physical parameters controlling the photorefractive effect in $KTa_{1-x}Nb_xO_3$:Cu,V

Victor Leyva, Aharon Agranat, and Amnon Yariv

Department of Applied Physics, California Institute of Technology, Pasadena, California 91125

Received March 1990; accepted August 15, 1990

We report photorefractive, absorption, and photoconductivity measurements made on a $KTa_{1-x}Nb_xO_3$:Cu,V sample after a series of reduction and oxidation treatments. All relevant physical parameters that enter into the Kukhtarev model of the photorefractive effect are determined. Photorefractive measurements are compared with those expected from theory. The oxidation–reduction process is modeled, which permits us to determine the heat treatment that is necessary to produce a given index change and response time. We discuss approaches to optimization of the photorefractive sensitivity.

1. INTRODUCTION

A great effort has gone into the development of photorefractive materials and the optimization of their properties. This effort has been motivated by the potential application of the photorefractive effect in such areas as optical computing, optical phase conjugation, and optical storage. Depending on the application, certain photorefractive properties of the material need to be optimized. These include the magnitude of the photorefractive-index change and the time and spectral response of the material. Of the metal oxides, the photorefractive properties of $LiNbO_3$,[1–4] $BaTiO_3$,[5–7] and $Sr_{1-x}Ba_xNb_2O_6$ (Ref. 8) have been extensively characterized over a wide range of experimental conditions. Properties were found to depend strongly on the presence of transition-metal dopants and on heat treatments. However, the nature of the photorefractive active species in many samples has not been determined. Even samples cut from the same boule can have widely varying properties. In addition, the difficulty of measuring parameters that enter into the Kukhtarev model[9,10] of the photorefractive effect has prevented careful comparison of experimental measurements with those expected from theory.

$KTa_{1-x}Nb_xO_3$ (KTN) is one of the first materials in which the photorefractive effect was observed.[11] One sample was shown to possess extremely high photorefractive sensitivity under two-photon illumination[12]; however, because of the scarcity of optical-quality samples little has been done to characterize its photorefractive properties. We previously reported the ability to control the magnitude of the photorefractive diffraction efficiency by using an externally applied field in a paraelectric KTN:Cu,V sample.[13] Recently we also reported results concerning the dependence of photorefractive properties on Cu valence-state concentrations in a KTN:Cu,V sample.[14] In this paper we investigate the photorefractive properties of a KTN:Cu,V sample by determining all physical parameters that are relevant to the Kukhtarev model. These parameters are determined through electron microprobe analysis, absorption measurements, and photoconductivity measurements. These results permit us to compare photorefractive diffraction and time response measurements after a series of reduction and oxidation treatments with those expected from the Kukhtarev model. We model the oxidation–reduction process, which enables us to determine the temperature and partial pressure of O_2 needed to produce a given photorefractive property. Finally, we discuss approaches to increasing the photorefractive sensitivity by controlling the dopant density and valence state.

2. EXPERIMENTAL RESULTS AND DISCUSSION

A. Sample Preparation and Treatments

We grew a 1.5 cm × 1.6 cm × 1.7 cm KTN:Cu,V crystal by using the top seeded solution growth method.[15] The flux contained an excess of K, to which 3 molar % of Cu and 3 molar % of V were added. V will be shown not to be the photorefractive active species. However, we found that a small percentage of V added to the flux acts as a solvent and results in significantly better-quality crystals.[16] A 0.52 cm × 0.41 cm × 0.31 cm sample was cut and polished along the principal crystallographic axis. Viewed through crossed polarizers, the sample appeared to be homogeneous and free of striations. Its chemical composition was determined by electron microprobe analysis to be $KTa_{0.70}Nb_{0.30}O_3$:Cu,V. Cu was found to be present at 600 parts in 10^6 by weight with a detection limit of 150 parts in 10^6. V was present at 40 parts in 10^6 with a detection limit of 15 parts in 10^6. The density of Cu is thus 1.80×10^{19} cm^{-3}, while that of V is 1.50×10^{18} cm^{-3}.

The ferroelectric phase-transition temperature of the KTN:Cu,V sample was determined from capacitance measurements to occur at roughly $T = -30$°C. An undoped KTN sample, used as a standard for the absorption measurements, was found to have a ferroelectric phase transition at $T = -32$°C. Since the transition temperature depends roughly linearly on Nb concentration,[17] the chemical composition of these two samples is nearly identical.

The KTN:Cu,V sample underwent a series of heat treatments in various O_2 atmospheres. After each treatment

0740-3224/91/030701-07$05.00

absorption, photoconductivity, and photorefractive measurements were made on the sample. For the first treatment the sample was sealed in an ampule containing 250 Torr (0.33 atm) of nominally pure Ar gas. The sample was then heated to 800°C and kept there for 15 h before cooling to room temperature. The other treatments consisted of sealing the sample in an ampule that contained 250 Torr of pure O_2. The ampule was then heated to a set temperature and kept there for 15 h before returning to room temperature. The temperatures used were 400, 450, 500, 600, and 700°C. The heating and cooling rates for all the treatments except the 700°C one were 75°C/h. The rates for the 700°C treatment were 180°C/h.

B. Absorption Measurements

After each heat treatment unpolarized absorption spectra were taken in the spectral range of 380–1100 nm with a double-beam spectrophotometer. The absorption coefficient α was determined from the relation

$$T = (1-R)^2 \exp(-\alpha l)/[1 - R^2 \exp(-2\alpha l)], \quad (1)$$

where l is the thickness of the sample, T is the measured transmission, and R is the reflection coefficient. R was determined by using the dispersion relationship for the index of refraction reported by Chen.[18]

Absorption mechanisms possible in the KTN samples include fundamental transitions and transitions that involve impurities and dopants. The fundamental absorption edge in KTN exhibits an Urbach dependence.[19] Absorptions that are due to transition-metal dopants are of two types, charge-transfer and crystal-field transitions. Charge-transfer transitions result in a free carrier, which can contribute to the photorefractive effect. Crystal-field transitions are due to localized transitions between d orbitals of the metal ion, split by an electrostatic interaction with the O ligands. Because they do not result in a free carrier, these transitions do not contribute to the photorefractive effect. Their characteristic absorption can be useful in identifying the presence, site occupancy, and valence state of transition-metal ions.[20]

The differences in the absorption spectra of the undoped KTN sample and the KTN:Cu,V sample after each of the reduction and oxidation treatments are shown in Fig. 1. Two absorption bands are visible. Since the KTN:Cu,V and the undoped KTN sample have approximately the same composition, features that are visible in the difference spectra should be a result of the dopants and not of the fundamental absorption. Because Cu is present in larger concentrations than V, its features should dominate the absorption spectra. Cu is stable in two valence states, Cu^{1+} and Cu^{2+}. Cu^{1+} has a filled $3d$ electronic shell; thus crystal field transitions are not allowed in this valence state. An electron charge-transfer transition, exciting an electron from Cu^{1+} into the conduction band, is possible. The band centered at 410 nm, which decreases in magnitude as oxidation treatment is increased, is identified as the electron charge-transfer band that is responsible for the photorefractive effect in our sample. The other stable Cu valence state is Cu^{2+}. The band centered at 680 nm is characteristic of crystal-field transitions of Cu^{2+} in an octahedrally coordinated site.[20] Cu^{2+} can also capture an electron that is photoexcited from the valence band, resulting in a free hole. In $LiNbO_3$:Cu, hole conductivity is observed[21] at energies above 3.6 eV. No evidence for this transition is found. The other dopant, V, is stable over a wide range of valence states. No absorption features characteristic of V are found.[22] Because it is isoelectronic with Ta and Nb, we expect it to enter the lattice in the V^{5+} state.

According to Beers' law, the intensity of these transitions is proportional to the concentration of absorbing ions. These two bands can thus be used to determine the relative concentration of Cu^{1+} and Cu^{2+} ions after each reduction and oxidation treatment.[21,23] Since the total concentration of Cu ions is known from the microprobe analysis, the absolute concentration of Cu in each valence state can be determined after each treatment. From Fig. 1 it is seen that after the reduction treatment the 680-nm band has disappeared. This result implies an almost complete conversion of the Cu to the Cu^{1+} valence state. An upper limit of ~1%, determined by the minimum discernible band at 680 nm, is determined for the Cu^{2+}/Cu ratio after this treatment. From the ratio of the peak magnitudes of the bands, the other treatments were found to convert 10, 18, 21, 27, and 36% of the Cu into the Cu^{2+} valence state.

An important parameter of photorefractive materials is the photoexcitation cross section, $s_e(\lambda)$. Along with the electronic recombination coefficient, it is the only parameter that enters into the Kukhtarev band transport model that is characteristic of the dopant. All other parameters are related to the host crystal or the concentration of the dopants. For many applications the dopant's spectral dependence determines its suitability as a photorefractive donor in the red and infrared regions. The spectral dependence given by

$$s_e(\lambda) = \alpha_{ct}/N, \quad (2)$$

where α_{ct} is the absorption coefficient of the transition that results in an electron's being excited into the conduction band and N is the concentration of absorbing ions. $s_e(\lambda)$ of Cu^{1+} in KTN:Cu,V can be determined from the

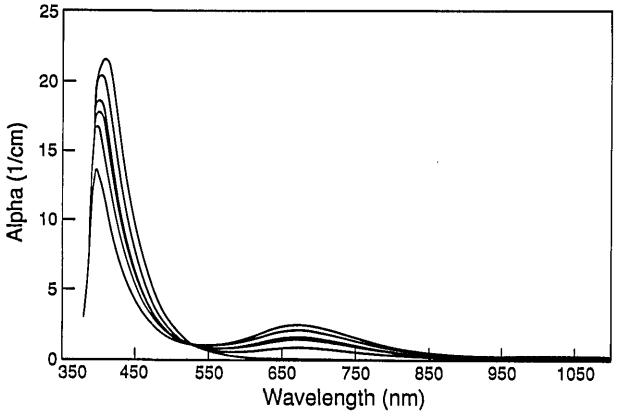

Fig. 1. Difference in absorption spectra between the undoped KTN sample and the KTN:Cu,V sample after a series of reduction and oxidation treatments. Features should be a result of the dopants. The spectrum with the largest magnitude at 410 nm corresponds to the reduction treatment. Other spectra with decreasing magnitudes at 410 nm correspond to the oxidation treatments at 400, 450, 500, 600, and 700°C.

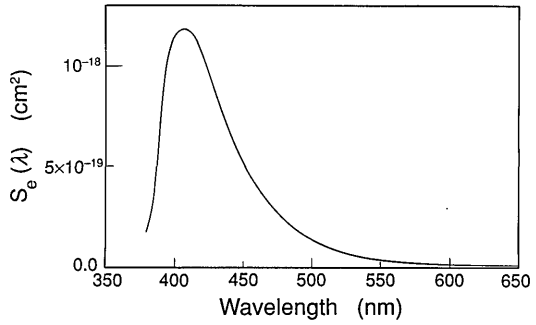

Fig. 2. Spectral dependence of the electron photoexcitation cross section, which results in an electron photoexcited from the Cu^{1+} ion into the conduction band. The peak at 3.0 eV corresponds to the optical excitation energy of this level.

difference absorption spectrum after the reduction treatment. For this spectrum almost all of the Cu is in the Cu^{1+} state, whose only allowed absorption results in a free electron. As is seen from Fig. 2, $s_e(\lambda)$ peaks at a value of 9.08×10^{-20} cm^2 at 410 nm and then drops sharply into the red. Cu, with an optical excitation energy of 3.0 eV below the conduction band, is not expected to show high photorefractive response in the red spectral region.

The excitation cross section for crystal-field transitions at 680 nm is found to be $s_{cf} = 1.5 \times 10^{-19}$ cm^2. This nonphotorefractive absorption is proportional to the concentration of Cu^{1+} ions. Both s_e and s_{cf} can be used as a standard to determine the concentration of Cu in each valence state for other Cu-doped KTN samples.

C. Photoconductivity Measurements

Photoconductivity measurements were made after each of the heat treatments in order to provide information on the transport parameters involved in the photorefractive effect. Under illumination the photocurrent is given by

$$J = e\mu(n_d + \tau_R \alpha_{ct} I/h\nu)E, \tag{3}$$

where e is the electronic charge, μ is the mobility, n_d is the free-electron density in the dark, τ_R is the electron recombination time, α_{ct} is the coefficient for absorption that results in a free carrier, I is the intensity, $h\nu$ is the energy of an incident photon, and E is the applied electric field. There is no photovoltaic effect in the paraelectric region.

After each of the reduction and oxidation treatments, the photocurrent was measured as a function of incident intensity and applied voltage. 514-nm illumination was used at intensities of 42–525 mW/cm^2 in 105 mW/cm^2 increments. Voltages from 200–1000 V in 200-V increments were applied along the 0.52-cm sides of the sample.

The sample was found to be highly insulating in the dark, which precluded measurements of the dark conductivity. The photocurrent was found to be linear in intensity and applied voltage. The mobility lifetime product, $\mu\tau_R$, was determined from the photocurrent by using the relation $\alpha_{ct} = s_e(514\text{ nm})[Cu^{1+}]$, where $s_e(514\text{ nm})$ was determined from Fig. 2. Figure 3 shows the dependence of $\mu\tau_R$ on Cu^{2+} concentration. It is seen to vary inversely with $[Cu^{2+}]$, the concentration of electron traps. This allows a determination of $[Cu^{2+}]/[Cu] = 0.0027$ for the reduction treatment, which we were unable to determine from the absorption measurements. τ_R is related to the electron recombination coefficient γ_R and to the trap concentration by

$$\tau_R = 1/\gamma_R[Cu^{2+}], \tag{4}$$

from which we determine $\mu/\gamma_R = 6.20 \times (10^8)$ 1/(V cm). From the experimentally determined inverse dependence of $\mu\tau_R$ on $[Cu^{2+}]$ and Eq. (4), we see that the mobility was relatively constant over the wide range of oxidation treatments. So any changes in the photorefractive properties after these treatments are due to changes in the valence states of the Cu ions and not to changes in the mobility.

D. Photorefractive Measurements

Photorefractive diffraction efficiency and erase-time measurements were made after each of the heat treatments. Measurements were made in the paraelectric region at $T = -27$°C. The sample was placed in a vacuum chamber on a thermoelectrically cooled mount. The dielectric constant was found from capacitance measurements to be $\epsilon = 12{,}000\epsilon_0$. An 800-V field was applied along the 0.52-cm sides. Two 514-nm beams intersecting at a 12° angle were used to write a grating with a 2.3-μm period. Each beam had an intensity of 42 mW/cm^2 and was expanded to illuminate the sample uniformly. The polarization was in the plane of incidence. The 0.31-cm-thick sample was exposed to the two beams for up to several minutes. One of the beams was then blocked. The diffracted intensity was measured as a function of time.

The absorption and photoconductivity measurements reveal that electrons are photoexcited from the Cu^{1+} level into the conduction band and are retrapped at the Cu^{2+} level. There is no evidence of hole conductivity or the existence of another species. Consequently the Kukhtarev band transport model with a single carrier and single species will be used to discuss our results. For small-intensity index modulation m, when we neglect the dark conductivity, the photorefractive space-charge field E_{sc} is given by[9,10]

$$E_{sc} = mE_q \frac{(E_0^2 + E_D^2)^{1/2}}{[(E_q + E_D)^2 + E_0^2]^{1/2}}, \tag{5}$$

where E_0 is the applied field, $E_D = k_B TK/e$ is the characteristic diffusion field, $E_q = eN_D{}^+(1 - N_D{}^+/N_D)/\epsilon K$ is the limiting space-charge field, K is the magnitude of the grating wave vector, N_D is the density of donors (total [Cu]

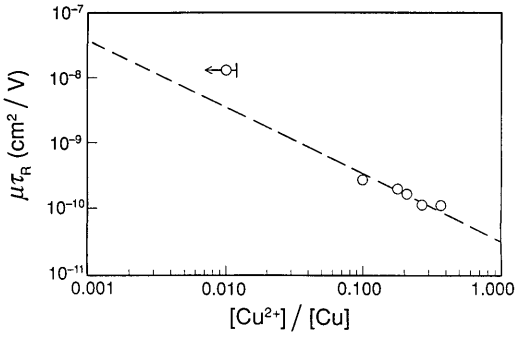

Fig. 3. Values of the mobility electron lifetime product, $\mu\tau_R$, versus trap concentration ratio. Trap concentration was varied through a series of reduction and oxidation treatments. The dashed line represents a linear fit to the data.

concentration), $N_D{}^+$ is the density of ionized donors ($[Cu^{2+}]$), and ϵ is the dielectric constant.

In the centrosymmetric paraelectric phase of KTN an external electric field E_0 is needed for production of an index grating that diffracts the incident beams. The index grating $\delta(\Delta n)$ is given by[13,24]

$$\delta(\Delta n) = n_0{}^3 g(\epsilon - \epsilon_0)^2 E_{sc} E_0, \tag{6}$$

where n_0 is the index of refraction and g the quadratic electro-optic coefficient. For KTN, $g_{11} = 1.36 \times (10^7)$ cm^4/C^2 and $n_0 = 2.34$ at 514 nm.[17] An expression for the diffraction efficiency, η, from an index grating written by two coupled waves is given by Kukhtarev.[9] For small coupling this simplifies to Kogelnik's expression for the diffraction efficiency from a plane, unslanted index grating given by[25]

$$\eta = \exp(-\alpha l)\sin^2\left[\frac{\pi\delta(\Delta n)l}{\lambda\cos(\theta/2)}\right], \tag{7}$$

where α is the total absorption, l is the thickness of the sample, λ is the wavelength of the illuminating radiation, and θ is the angle between the writing beams.

The photorefractive response time τ_e under an applied field, when we neglect the dark conductivity, is given by[9,10]

$$\tau_e = \tau_{di}\frac{(1 + \tau_R/\tau_D)^2 + (\tau_R/\tau_E)^2}{[1 + \tau_R\tau_{di}/(\tau_D\tau_I)](1 + \tau_R/\tau_D) + (\tau_R/\tau_E)^2(\tau_{di}/\tau_I)}, \tag{8}$$

where

$$\tau_{di} = \frac{\epsilon}{\epsilon\mu n_d}, \tag{9a}$$

$$\tau_E = \frac{1}{K\mu E_0}, \tag{9b}$$

$$\tau_D = \frac{e}{\mu k_B T K^2}, \tag{9c}$$

$$\tau_R = \frac{1}{\gamma_R N_D{}^+}, \tag{9d}$$

$$\tau_I = \frac{1}{sI/h\nu + \gamma_R n_0}, \tag{9e}$$

and

$$n_d = \frac{sI(N_D - N_D{}^+)}{h\nu\gamma_R N_D{}^+} \tag{9f}$$

is the free-electron density.

From the electron microprobe, absorption, and photoconductivity measurements, we determined values for all the parameters involved in Eqs. (5) and (8). These include the density of filled and ionized donors after each of the heat treatments, the electron photoexcitation cross section, and the ratio of the electron mobility to the recombination rate. This permits us to compare our experimental results with those expected from the Kukhtarev model.

The experimental results for the diffraction efficiency versus the trap density, as well as that expected from the Kukhtarev model, are given in Fig. 4. The diffraction efficiency is defined as the ratio of the incident to the diffracted intensity. The zeros in the theoretical plot occur for increasing index change when the argument of the sine function in Eq. (7) is an integral multiple of π. Experimentally measured index changes are much smaller than those expected from theory. Measured index changes are never large enough to reach the first zero. For the reduction treatment, $[Cu^{2+}]/[Cu] = 0.0027$, the diffraction efficiency is 0.81%. All the other oxidation treatments resulted in a fairly constant diffraction efficiency of ~13%. Beam fanning was in a direction consistent with electron conductivity. Both the model and the experiment show an index change that is nearly independent of the trap density in the space-charge limiting region, $E_q \gg (E_0, E_D)$. This occurs roughly for $[Cu^{2+}]/[Cu] > 0.10$.

The lower measured index changes may be a result of several factors. As previously mentioned, Eq. (7) is a small-coupling approximation. Good agreement, however, is expected under the conditions of drift mode writing in a thin 3-mm-thick grating. The largest discrepancy is expected from the violation of the small-modulation approximation that was used to derive Eq. (8). Refregier *et al.* showed that nonlinear terms in m modify the space-charge field.[26] For large values of m these lead to a smaller index change than expected from Eq. (8). We also assumed that the applied voltage across the sample resulted in a uniform electric field. The sample was illuminated uniformly to ensure this, but regions of large voltage drops may have occurred at or near the electrodes. Photorefractive beam fanning is expected to result in a large discrepancy between model and experiment. We expect this loss mechanism to result in a decrease in the magnitude of the space-charge field and measured diffraction efficiency. Until it can be taken into account, poor agreement between the two is expected.

The dependence of the experimentally measured erase times on trap density and that expected from Eq. (9) are shown in Fig. 5. The erase time τ_e was found by fitting an exponential decay to $\delta(\Delta n)$. The decay of $\delta(\Delta n)$ during readout was determined from the diffracted intensity with Eq. (7). The erase times under 42-mW/cm^2 illumination varied from 0.60 to 138 sec. Reasonable agreement is found with Eq. (11), although the measured times are slightly lower.

E. Reduction and Oxidation of Cu

The reduction and oxidation treatments altered the Cu valence-state concentrations and photorefractive proper-

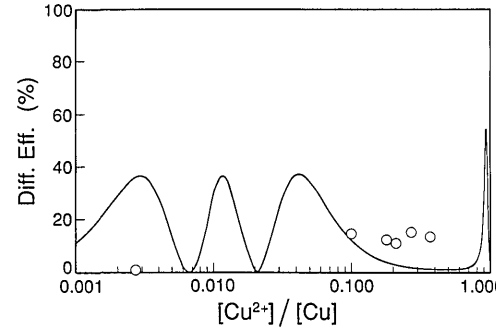

Fig. 4. Experimentally measured diffraction efficiencies from a photorefractive grating versus trap concentration ratio, circles, and that expected from the Kukhtarev model, curve, in paraelectric KTN:Cu,V. All parameters arising in the model were measured independently of photorefractive measurements.

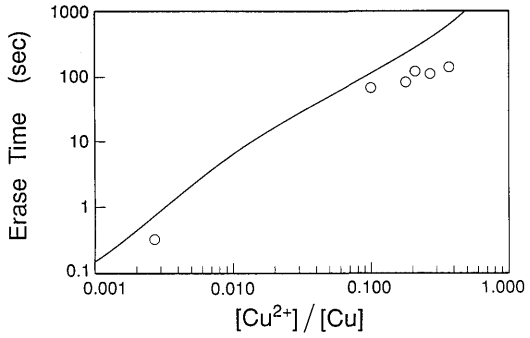

Fig. 5. Expèrimentally measured erase rates of a photorefractive grating during readout, circles, and that expected from the Kukhtarev model, curve, versus trap concentration ratio. Erase rates are for a 42-mW/cm^2, 514-nm readout beam.

ties of the sample over a wide range. The reduction and oxidation treatments induce changes in the Cu valence through the creation of O vacancies.[4,27] When heated in an O_2-deficient atmosphere, O vacancies are induced in the sample. The two electrons paired with the O site can remain free or be trapped at the vacancy site or by a multivalent metal ion. The oxidation process is given by

$$Cu^{1+} + \tfrac{1}{2}V_O + \tfrac{1}{4}O_2 \rightarrow Cu^{2+}, \tag{10}$$

where V_O represents an oxygen vacancy and O_2 an oxygen gas molecule. From EPR measurements,[28] Cu is expected to enter the Ta or Nb site substitutionally. O vacancies are relatively shallow and should be ionized at room temperature. Charge neutrality relative to the neutral lattice is given by

$$4[Cu^{1+}] + 3[Cu^{2+}] + n = 2[V_O] + p, \tag{11}$$

where n is the free-electron concentration and p is the free-hole concentration. A mass-action equation[29] can be used to determine the concentration of the components of reaction (10) in equilibrium:

$$[Cu^{1+}][V_O]^{1/2}P_{O_2}{}^{1/4}/[Cu^{2+}] = K\exp(\Delta H/kT), \tag{12}$$

where ΔH is the change in enthalpy of the reaction, K is a constant, and P_{O_2} is the partial pressure of oxygen at the processing temperature. The values of $[Cu^{1+}]$, $[Cu^{2+}]$, and P_{O_2} are known for each of the heat treatments. By neglecting the free-electron and free-hole concentrations, Eq. (11) can be used to determine $[V_O]$. In Fig. 6 the value of the left-hand side of Eq. (12) is plotted versus the inverse processing temperature. As noted in Subsection 2.A, a faster heating and cooling rate was used for the 700°C treatment. The good agreement of the fitted line with the data points implies that the cooling rates were fast enough to prevent a change in the Cu valence concentrations on cooling. A value of $K = 1.48 \times 10^{19}$ Torr$^{1/4}$ cm$^{-3/2}$ (2.83×10^{18} atm$^{1/4}$ cm$^{-3/2}$) and $\Delta H = 0.295$ eV is determined from Fig. 6. These values permit us to determine the required temperature and partial pressure of O_2 that is needed to adjust the Cu valence-state concentrations. In Fig. 7 we show the Cu^{2+} fraction versus the partial pressure of O_2 at a processing temperature of 700°C for various doping levels. For a given O_2 partial pressure, lower doping levels are seen to result in a higher fraction of filled donors, Cu^{1+}.

ΔH is given by half the energy needed to fill the vacancy site with an O ion and two free electrons minus the energy needed to thermally ionize an electron from Cu^{1+} to the conduction band. For an ionic solid, no energy is necessary to place a neutral O ion in the vacancy site. Since the valence band consists of O $2p$ orbitals, the energy needed to place two free electrons in the neutral O site is twice the band-gap energy. The band-gap energy was found from the absorption measurements to be $E_{gap} = 3.25$ eV. The thermal energy of the Cu^{1+} donor level is thus determined to be $E_{Cu^{1+}} = 2.95$ eV below the conduction band. Note that this is slightly less than the peak in the optical excitation energy of 3.00 eV (Fig. 2). As was pointed out by Mott,[30] the thermal energy is always the smaller of the two because of lattice movements.

3. OPTIMIZING THE PHOTOREFRACTIVE EFFECT

In this paper we have shown how reduction and oxidation treatments can significantly alter the magnitude of the photorefractive-index change and response time. A parameter useful in comparing the photorefractive properties of samples is the photorefractive sensitivity S.[10] It is defined as the index change per absorbed energy per unit volume. Assuming an exponential decay of the index grating with a time constant of τ_e, S is given in paraelectric KTN:Cu,V by

$$S = \frac{d(\Delta n)}{d(\alpha I \tau_e)} = \frac{n_0{}^3 g(\epsilon - \epsilon_0)^2 E_{sc} E_0}{s_e[Cu^{1+}] I \tau_e}, \tag{13}$$

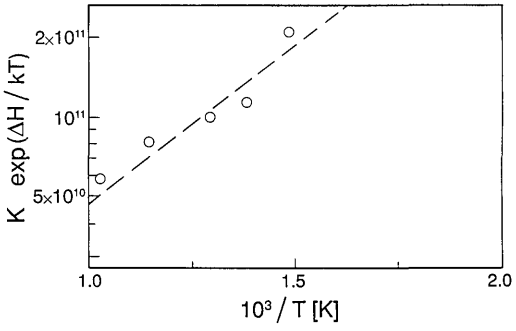

Fig. 6. Plot of the left-hand side of the mass action equation (12) for the oxidation–reduction process versus inverse temperature. The dashed line corresponds to $K = 1.48 \times 10^{19}$ Torr$^{1/4}$ cm$^{-3/2}$ [2.83×10^{18} atm$^{1/4}$ cm$^{-3/2}$] and $\Delta H = -0.295$ eV.

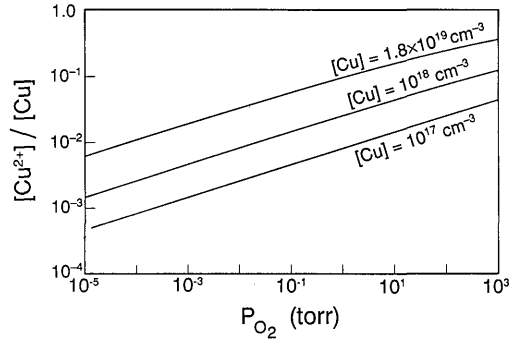

Fig. 7. Fraction of the Cu in the Cu^{2+} valence state versus partial pressure of O_2 at a processing temperature of 700°C. Three doping levels are shown: [Cu] of 1.8×10^{19} cm^{-3}, 10^{18} cm^{-3}, and 10^{17} cm^{-3}.

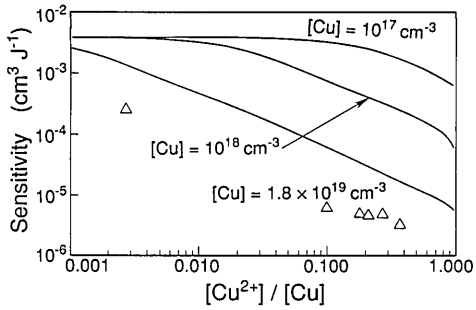

Fig. 8. Experimentally measured photorefractive sensitivity versus trap concentration ratio. Also plotted is the sensitivity expected from theory for three different doping levels.

where all parameters have been defined. Note that E_{sc} depends on E_0, ϵ, and the concentration of Cu^{1+} and Cu^{2+}. In Fig. 8 the sensitivity of the sample after each of the heat treatments is plotted versus the $[Cu^{2+}]/[Cu]$ concentration ratio. The index change Δn was determined from the diffraction efficiency measurements with Eq. (7). Also plotted is the sensitivity expected from theory for three different doping levels. Values for the material parameters and the experimental conditions are similar to those used above. The experimental points correspond to the $[Cu] = 1.8 \times 10^{19}\ cm^{-3}$ curve. Measured values are approximately an order of magnitude lower than those expected from theory. A significant improvement in S is found for reduced samples, i.e., those with a low trap concentration. From Fig. 7 we see that, for a given processing temperature and oxygen partial pressure, lower-doped samples are more highly reduced. These factors may explain why high sensitivities have been reported in nominally undoped samples compared with those in heavily doped ones.

Approximating τ_e with the dielectric relaxation time simplifies Eq. (13) to

$$S = \frac{4\pi e n_0^3 g \epsilon E_{sc} E_0 \mu}{h\nu\gamma[Cu^{2+}]}, \tag{14}$$

where use has been made of $\epsilon \gg \epsilon_0$.

S is found to be proportional to the mobility μ. The mobility is a property of the host material and in our sample was found to be unaffected by the heat treatments. In order to determine approaches to optimization of the sensitivity, two limiting cases can be considered. In the space-charge limiting case, $E_{sc} \sim E_q = e[Cu^{2+}][Cu^{1+}]/\epsilon K[Cu]$, S is linearly dependent on the applied field and on the ratio $[Cu^{1+}]/[Cu]$. This ratio can be increased through reduction treatments. S is also independent of the strongly temperature-dependent dielectric constant, so no improvement is expected from cooling the sample closer to the phase transition. In the second case, where $E_q \gg (E_0, E_D)$, the field varies as $E_{sc} \sim (E_0^2 + E_D^2)^{1/2}$. S is now inversely proportional to the trap concentration $[Cu^{2+}]$ and is more strongly dependent on applied field. Also, S is proportional to ϵ and can be increased by cooling the sample to a temperature near the ferroelectric phase transition. Generally the sensitivity is improved when the carrier is transported large distances before it is trapped. Therefore large applied fields and low trap concentrations, achieved through reduction heat treatments, are needed.

4. SUMMARY

In summary, we have presented an investigation of the material parameters that are involved in the photorefractive effect in KTN:Cu,V. After a series of oxidation and reduction treatments, electron microprobe analysis and absorption and photoconductivity measurements are used to determine all the material parameters that enter into the Kukhtarev model of the photorefractive effect. These include the filled and the ionized electron donor concentrations, the electron photoexcitation cross section, and the ratio of the electron mobility to the recombination rate. These determinations permit us to compare photorefractive measurements with those expected from theory. Good agreement is found for the photorefractive erase-time measurements, but the magnitude of the index change is smaller than expected. We model the oxidation–reduction process, which permits us to determine the temperature and partial pressure of O_2 needed to yield given filled and ionized donor concentrations. The energy level of the Cu^{1+} is found to agree closely with the optical excitation energy. We conclude by discussing approaches to increasing the photorefractive sensitivity.

ACKNOWLEDGMENTS

This research is supported by the U.S. Army Research Office. V. Leyva acknowledges the support of an AT&T Graduate Fellowship.

REFERENCES

1. G. E. Peterson, A. M. Glass, and T. J. Negran, "Control of the susceptibility of lithium niobate to laser-induced refractive index changes," Appl. Phys. Lett. **19,** 130–132 (1971).
2. W. Phillips, J. J. Amodei, and D. L. Staebler, "Optical and holographic properties of transition metal doped lithium niobate," RCA Rev. **33,** 94–109 (1972).
3. M. Clark, F. DiSalvo, A. M. Glass, and G. Pearson, "Electronic structure and optical index damage of iron-doped lithium niobate," J. Chem. Phy. **59,** 6209–6219 (1973).
4. W. Phillips and D. L. Staebler, "Control of the Fe^{2+} concentration in iron-doped lithium niobate," J. Electron. Mater. **3,** 601–616 (1974).
5. M. B. Klein and G. C. Valley, "Beam coupling in $BaTiO_3$ at 442 nm," J. Appl. Phys. **57,** 4901–4905 (1985).
6. S. Ducharme and J. Feinberg, "Altering the photorefractive properties of $BaTiO_3$ by reduction and oxidation at 650°C," J. Opt. Soc. Am. B **3,** 283–292 (1986).
7. M. B. Klein and R. N. Schwartz, "Photorefractive effect in $BaTiO_3$: microscopic origins," J. Opt. Soc. Am. B **3,** 293–305 (1986).
8. G. Rakuljic, A. Yariv, and R. Neurgaonkar, "Photorefractive properties of undoped, cerium-doped, and iron-doped single-crystal $Sr_{0.6}Ba_{0.4}Nb_2O_6$," Opt. Eng. **25,** 1212–1216 (1986).
9. N. V. Kukhtarev, V. B. Markov, S. G. Odulov, M. S. Soskin, and V. L. Vinetski, "Holographic storage in electrooptic crystals. I. Steady state," Ferroelectrics **22,** 949–960 (1979).
10. G. C. Valley and M. B. Klein, "Optimal properties of photorefractive materials for optical data processing," Opt. Eng. **22,** 704–711 (1983).
11. F. S. Chen, "A laser-induced inhomogeneity of refractive indices in KTN," J. Appl. Phys. **38,** 3418–3420 (1967).
12. D. von der Linde, A. M. Glass, and K. F. Rodgers, "High sensitivity optical recording in KTN by two-photon absorption," Appl. Phys. Lett. **26,** 22–24 (1975).
13. A. Agranat, V. Leyva, and A. Yariv, "Voltage-controlled photorefractive effect in paraelectric $KTa_{1-x}Nb_xO_3$:Cu,V," Opt. Lett. **14,** 1017–1019 (1989).
14. V. Leyva, A. Agranat, and A. Yariv, "Dependence of the photorefractive properties of $KTa_{1-x}Nb_xO_3$:Cu,V on Cu valence state concentration," J. Appl. Phys. **67,** 7162–7165 (1990).

15. A. Agranat, V. Leyva, K. Sayano, and A. Yariv, "Photorefractive properties of $KTa_{1-x}Nb_xO_3$ in the paraelectric phase," Proc. Soc. Photo-Opt. Instrum. Eng. **1148,** 52–66 (1989).
16. P. Bohac and H. Kaufmann, "KTN optical waveguides grown by liquid-phase epitaxy," Electron. Lett. **22,** 861–862 (1986).
17. S. Triebwasser, "Study of ferroelectric transitions of solid-solution single crystals of $KNbO_3$-$KTaO_3$," Phys. Rev. **114,** 63–70 (1959).
18. F. S. Chen, J. Geusic, S. Kurtz, J. Skinner, and S. Wemple, "Light modulation and beam deflection with potassium tantalate-niobate crystals," J. Appl. Phys. **37,** 388–398 (1966).
19. Y. Brada and M. Roth, "Optical absorption of $KTa_{1-x}Nb_xO_3$ single crystals," Phys. Rev. B **39,** 10402–10405 (1989).
20. G. Rossman, "Optical spectroscopy," Rev. Mineralogy **18,** 207–254 (1988).
21. E. Kratzig and R. Orlowski, "Light induced transport in doped $LiNbO_3$ and $LiTaO_3$," Ferroelectrics **27,** 241–244 (1980).
22. K. Schmetzer, "Absorptionsspektroskopie und Farbe von V^{3+}-haltigen naturlichen Oxiden und Silikaten—ein Beitrag zur Kristallchemie des Vanadiums," Neues Jahrb. Mineral. Abh. **144,** 73–106 (1982).
23. E. Kratzig and R. Orlowski, "$LiTaO_3$ as holographic storage material," Appl. Phys. **15,** 133–139 (1978).
24. R. Orlowski, L. A. Boatner, and E. Kratzig, "Photorefractive effects in the cubic phase of potassium tantalate-niobate," Opt. Commun. **35,** 45–48 (1980).
25. H. Kogelnik, "Coupled wave theory for thick hologram gratings," Bell Syst. Tech. **48,** 2909–2947 (1969).
26. Ph. Refregier, L. Solymar, H. Rajbenbach, and J. P. Huignard, "Two-beam coupling in photorefractive $Bi_{12}SiO_{20}$ crystals with moving grating: theory and experiments," J. Appl. Phys. **58,** 45 (1985).
27. B. A. Wechsler and M. B. Klein, "Thermodynamic point defect model of barium titanate and application to the photorefractive effect," J. Opt. Soc. Am. B **5,** 1711–1723 (1988).
28. L. A. Boatner, A. Kayal, and U. T. Hochli, "Electronic properties of pure and Cu-doped $KTaO_3$," Helv. Phys. Acta **50,** 167–169 (1977).
29. F. Rosenberger, *Fundamentals of Crystal Growth I* (Springer-Verlag, Berlin, 1979).
30. N. F. Mott and R. W. Gurney, *Electronic Processes in Ionic Crystals* (Dover, New York, 1964).